Lab on a Chip

Accepted Manuscript

ROYAL SOCIETY OF CHEMISTRY

www.rsc.org/loc

Lab on a Chip

RSCPublishing

ARTICLE

Dual-pore glass chips for cell-attached single-channel recordings†‡

Cite this: DOI: 10.1039/x0xx00000x

Brandon R. Bruhn[a], Haiyan Liu[a], Stefan Schuhladen[a], Alan J. Hunt[a], Aghapi Mordovanakis[a,b] and Michael Mayer[a,c]

Received 00th February 2014,
Accepted 00th February 2014

DOI: 10.1039/x0xx00000x

www.rsc.org/

While high-throughput planar patch-clamp instruments are now established to perform whole-cell recordings for drug screening, the conventional micropipette-based approach remains the gold standard for performing cell-attached single-channel recordings. Generally, planar platforms are not well-suited for such studies due to excess noise resulting from low seal resistances and the use of substrates with poor dielectric properties. Since these platforms tend to use the same pore to position a cell by suction and establish a seal, biological debris from the cell suspension can contaminate the pore surface prior to seal formation, reducing the seal resistance. Here, femtosecond laser ablation was used to fabricate dual-pore glass chips optimized for use in cell-attached single-channel recordings that circumvent this problem by using different pores to position a cell and to establish a seal. This dual-pore design also permitted the use of a relatively small patch aperture (D ~ 150 to 300 nm) that is better-suited for establishing high-resistance seals than the micropores used typically in planar patch-clamp setups (D ~ 1 to 2 μm) without compromising the ability of the device to position a cell. Taking advantage of the high seal resistances and low capacitive and dielectric noise realized using glass substrates, patch-clamp experiments with these dual-pore chips consistently achieved high seal resistances (rate of gigaseal formation = 61%, mean seal resistance = 53 GΩ), maintained gigaseals for prolonged durations (up to 6 hrs), achieved RMS noise values as low as 0.46 pA at 5 kHz bandwidth, and enabled single-channel recordings in the cell-attached configuration that are comparable to those obtained by conventional patch-clamp.

Introduction

Ion channels comprise a diverse family of tightly regulated, pore-forming membrane proteins that permit the passive transport of ions across biological membranes and play a vital role in signal transduction and gene transcription, among other functions.[1] More than 50 different disorders (*i.e.* channelopathies) such as cystic fibrosis and epilepsy are known to result from mutations in genes encoding for ion channels. Moreover, ion channel dysfunction is involved in many other conditions such as hypertension and chronic pain.[2,3] Consequently, drugs that target ion channels account for more than 13 percent of the pharmaceutical market, making ion channels the second most targeted family of proteins behind G protein-coupled receptors.[4] Nevertheless, ion channels are still underutilized as drug targets in part due to inadequate target validation and a dependence on *indirect* screening technologies (*e.g.* fluorescence-based assays).[5]

The patch-clamp technique has remained the gold standard for *directly* screening ion channel activity since its invention by Erwin Neher and Bert Sakmann in the 1970s.[6,7] In a conventional patch-clamp experiment, the tip of a fire-polished, glass micropipette (D ~ 1 to 2 μm) is carefully positioned in contact with an adherent cell and gentle suction is applied to establish a high-resistance seal between the micropipette and cell membrane (Fig. 1a). The electrical resistance of the seal is inversely proportional to background noise (*i.e.* Johnson and shot noise) and therefore must be sufficiently large (typically ≥ 1 GΩ) to distinguish ion channel activity from noise.[8] In a whole-cell recording, the membrane patch encompassed by the micropipette tip is ruptured to provide electrical access to the interior of the cell and a high-gain amplifier records the ensemble average of all ion channel activity *via* electrodes in the electrolyte-filled pipette and bath solution. Conversely, in a cell-attached single-channel recording, the membrane patch is kept intact to record the activity of only those ion channels in the electrically isolated region of membrane. Unlike whole-cell recordings, single-channel recordings permit detailed kinetic analyses of individual ion channels, allow related or mutated channels to be distinguished based on their unitary conductances or their open-state and closed-state probabilities, and enable the investigation of drug-ion channel interactions at

the single-molecule level.[2,9] Whole-cell and single-channel recordings each provide valuable yet complementary information that is critical for understanding ion channel behavior and selecting viable drug targets.

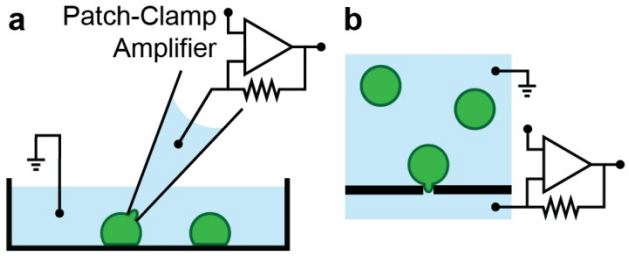

Fig. 1 Illustration of (**a**) conventional and (**b**) planar patch-clamp recordings. In a planar patch-clamp recording, a microfabricated pore replaces the micropipette used in a conventional recording.

Despite its widespread use, conventional patch-clamp is a low-throughput technique (tens of data points per day) that requires highly trained personnel and expensive equipment such as a micromanipulator and optical microscope[6]. As a result, automated patch-clamp platforms have been developed to enable multiple recordings in parallel. Planar patch-clamp platforms are the most common variety; here, a micropore in a planar substrate is used to patch a cell from suspension (Fig. 1b). Borosilicate glass and quartz substrates typically provide the highest rates of GΩ seal (*i.e.* gigaseal) formation[10–14], though various other materials have been used, including silicon coated with SiO_2 or phosphosilicate glass (PSG)[15–25], PEG/SU-8[26], PDMS[27–30], polyimide[31,32], and a cyclic olefin copolymer (COC)[33]. While planar patch-clamp platforms offer low-cost, high-throughput electrophysiological data with up to 18,000 data points per day, these devices seldom obtain seal resistances that are comparable to the conventional micropipette-based technique and are largely limited to whole-cell recordings in which the signal-to-noise ratio is high.[10,34,35] The inability of these devices to perform cell-attached single-channel recordings reliably is exemplified by the scarcity of published papers that demonstrate such recordings on an automated platform.[10,11,28,36]

Here, we used femtosecond laser ablation to fabricate dual-pore glass chips optimized for use in cell-attached single-channel recordings. The dual-pore design is similar to that of the CytoPatch chip by Cytocentrics, wherein one pore (*i.e.* the positioning pore) positions a cell by suction while another nearby pore (*i.e.* the recording pore) avoids contamination by maintaining positive pressure until a cell is positioned and then establishes a seal.[15] Other planar patch-clamp platforms typically use the same pore to position a cell and establish a seal, hence increasing the chance of contaminating the pore surface with biological debris from the cell suspension prior to seal formation, which reduces the seal resistance. In contrast to the CytoPatch chip, however, the chips developed here are made of borosilicate glass; this material generally yields higher seal resistances and has lower dielectric and capacitive current noise than SiO_2 on silicon.[10] Furthermore, the recording pore is smaller in diameter (150 to 300 nm instead of ~1.5 μm), which is advantageous for forming high-resistance seals.[8] Such a small pore would not be practical in a standard one-pore design as it would make it difficult to position a cell due to its high resistance to fluid flow. Our design takes inspiration from conventional patch-clamp, wherein smaller patch pipette openings are generally used for cell-attached recordings in comparison to those used for whole-cell recordings.[8] Patch-clamp experiments with these dual-pore chips consistently achieved high seal resistances (≥ 10 GΩ), maintained gigaseals for prolonged durations (up to 6 hrs), and enabled cell-attached single-channel recordings that are comparable to those obtained by conventional patch-clamp.

Experimental

Machining setups

To machine the recording and positioning pores (Fig. 2a-b), we used a diode-pumped Nd:glass chirped-pulse amplification laser system (Intralase) to generate 600-fs-long pulses at a wavelength of 1053 nm that were later frequency doubled by a KTP crystal to clean their temporal and spatial profile. We used a photodiode to measure the average power of the laser, which we adjusted with a reflective variable-density filter. We directed the laser into the epifluorescence path of an Axiovert 200M inverted microscope (Zeiss) and used a 40x, 0.65 NA Achroplan air objective (Zeiss) to focus the laser into a 150-μm-thick, borosilicate glass coverslip (72228, Electron Microscopy Sciences). We used a piezoelectric positioner (P-725.1CL, Physik Instrumente) to control the focal plane of the objective and an xy-nanostage (PI-629.2CL, Physik Instrumente) to move the coverslip laterally with respect to the focal spot. We put Milli-Q water on top of the coverslip and a solution containing 2 M KCl underneath to enhance debris removal[37] from the pores and to monitor the electrical connectivity across the chip with a picoammeter/voltage source (6487, Keithley). Last, we used custom-written MATLAB (MathWorks) software to interface with the various electronics described here *via* a data acquisition board (PCI-6259, National Instruments). Supplementary Section S1 shows a simplified schematic of this machining setup.

We used a similar setup to machine channels on the surface of the coverslip for interfacing with each pore (Fig. 2c). Here, we used a fiber laser (Satsuma, Amplitude Systems) to generate 400-fs-long pulses at a wavelength of 1030 nm. To generate a relatively large focal volume, we focused the laser into the substrate with a 20x, 0.50 NA Achroplan air objective (Zeiss). We used the motorized focusing drive of an Axiovert 200M inverted microscope (Zeiss) to control the focal plane of the objective and an xy-microstage (BioPrecision2, Ludl) to move the coverslip laterally. In addition, we controlled the lateral position of the focal spot by adjusting the angle of two scanning galvo mirrors (GVS012, Thorlabs). As with the other setup, we kept Milli-Q water above the chip to enhance debris removal and used Matlab to interface with the electronics.

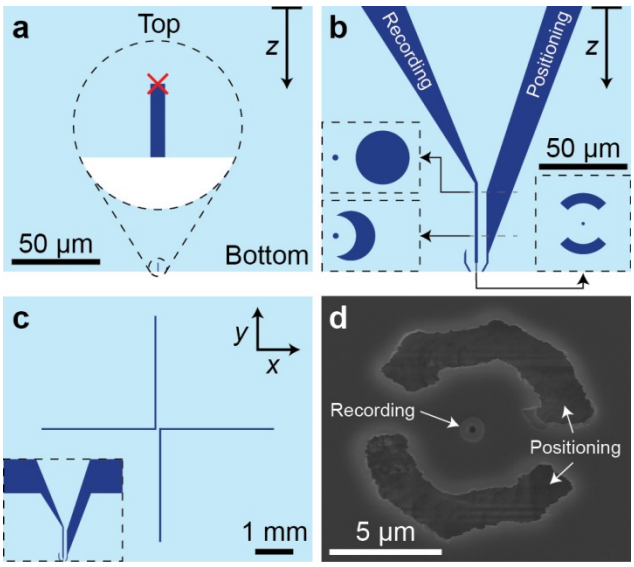

Fig. 2 Major stages in the fabrication of a dual-pore glass chip. (**a**) Illustration showing a vertical cross-section after using a single femtosecond pulse to machine the aperture used for establishing seals. The red 'x' indicates the approximate focal depth of the laser. The diameter of the aperture varies between 150 to 300 nm. (**b**) Same cross-section shown in pane (a) after using high-repetition-rate femtosecond laser ablation to machine the remainder of the recording pore (left) and entirety of the positioning pore (right). At the top surface, the pores are 20 µm in diameter and spaced by 100 µm from center to center. Moving downward, the pores steadily decrease in diameter and approach one another until the recording pore is centered above the single-shot aperture on the bottom surface ($z \approx 100$ µm). As z further increases, the positioning pore continues to decrease in diameter as it gradually encircles the recording pore, which remains fixed at 1.6 µm in diameter (see left insets). A 5-µm-thick layer of glass separates the pores in this region. Once the positioning pore is centered about the recording pore ($z \approx 140$ µm), the positioning channel splits into two segments (see right inset) to avoid fracturing the wall that separates the pores. Each subsequent layer is identical until the upper portion of the recording pore intersects the single-shot aperture, whereupon the distance between the two pores gradually decreases. At the bottom surface (right inset), the inner and outer diameters of the positioning pore are typically 6 and 8 µm, respectively. (**c**) Top view after using high-repetition-rate ablation to machine low-resistance channels on the surface of the glass for interfacing electrically and fluidically with each pore. Each segment of the L-shaped channels is 3 mm long, 45 µm wide, and 50 µm deep. The pores are located at the vertices of the L-shaped channels. The inset shows a vertical cross-section. (**d**) SEM image of the bottom surface. All panes are drawn to scale.

Fabrication procedure

To machine the recording and positioning pores (Fig. 2a-b), we first ablated the opening of the recording pore on the bottom side of the coverslip by focusing a single femtosecond pulse as deep into the glass as possible while still yielding visible damage (Fig. 2a). To yield a relatively long aperture, we used a laser power that was two times larger than the single-shot ablation threshold as measured on the top surface (see Supplementary Section S2 for details). Next, we used high-repetition-rate (2 kHz) femtosecond laser ablation to machine the remainder of the recording pore and the entirety of the positioning pore layer by layer from top to bottom (Fig. 2b). We machined each layer by scanning the laser focus no faster than 150 µm s^{-1} (corresponding to 1 pulse per 75 nm) along circular or semi-circular trajectories that are evenly spaced in the radial direction and centered about each pore. While machining the upper 100 µm of the coverslip, we used a laser power that was 25 percent above the high-repetition-rate threshold as measured on the top surface (see Supplementary Section S2) and a radial step size of 1 µm. We limited the vertical step size (*i.e.* spacing between layers) to a maximum of 1 µm and gradually decreased its value such that the ablated regions in adjacent layers overlapped by at least 90 percent in terms of area. Once the positioning pore started to encircle the recording pore (Fig. 2b, left insets), we began ablating each layer of the positioning pore twice and reduced the laser power to 10 percent above threshold as measured on the bottom surface (see Supplementary Section S2) and reduced the radial and vertical step sizes to 0.2 and 0.4 µm, respectively. Once the positioning pore was centered about the recording pore, we resumed ablating each layer only once. We halted machining of the recording pore once the current increased by 0.2 nA at an applied potential of 500 mV. Machining of the positioning pore continued until the focal plane was positioned below the bottom surface of the chip. This procedure took approximately 45 minutes to complete. Immediately following ablation, we placed the coverslip in Milli-Q water with its upper surface (Fig. 2b) facing downward to allow additional debris to settle out of the pores.

We used high-repetition-rate (200 kHz) ablation to machine low-resistance L-shaped microchannels for interfacing with each pore (Fig. 2c). As before, machining proceeded layer by layer from top to bottom. We used a laser power that was roughly twice that of the high-repetition-rate threshold as measured on the top surface (see Supplementary Section S2) and a vertical step size of roughly 2 µm. We machined each layer by scanning the laser focus about the length of each channel at a rate of 200 µm s^{-1}. Simultaneously, we oscillated a galvo mirror at 100 Hz to quickly move the laser focus back-and-forth along the channel width. To account for tilt in the coverslip, we discretely adjusted the position of the objective along the length of the channel each time the position of the surface changed by more than 0.5 µm (see Supplementary Section S3 for details). This procedure took approximately 20 minutes to complete.

We optimized all parameters to minimize the failure rate of the machining process and to prevent cracking of the glass substrate; for instance, excessive laser power results in the formation of microcracks in the vicinity of the ablated structures. Following laser fabrication, we often etched the chips for a short duration ($\leq$ 30 s) in a buffered hydrofluoric acid solution (Buffer HF Improved, Transene) to remove residual debris from the pores.

Cell culture

HEK-293 cells transfected with large-conductance Ca^{2+}-activated K^+ (BK) channels were obtained from Dr. Heike Wulff (University of California, Davis) and were cultured in Dulbecco's modified Eagle medium (DMEM, ATCC) with 10% (v/v) fetal bovine serum (Gibco), 0.5 mg/mL G418 (Sigma-Aldrich), 100 units/mL penicillin (Gibco), and 100 µg/mL streptomycin (Gibco). To prepare these cells for patching, we first rinsed the cell culture flask in PBS to remove extracellular

proteins. Next, we treated the cells with 0.05% (w/v) trypsin-EDTA (Gibco) for 3 minutes at 37 ºC, adding fresh medium to stop the trypsinization process. We then aspirated and centrifuged the suspension. We resuspended the cells in cell culture medium and waited 15 minutes as we measured the cell density. Subsequently, we centrifuged the suspension and resuspended the cells in an electrolyte solution (see "Patch-clamp experiments" subsection) to achieve a density of roughly 10^6 cells mL^{-1}. We passed the suspension through a 40 µm cell strainer (Becton Dickinson) to remove cell aggregates. Last, we placed the suspension in a 1 mL Eppendorf tube, which was constantly mixed at 800 rpm and 37 ºC *via* a Thermomixer R (Eppendorf). This procedure has been shown to reduce the number of cell aggregates and to maintain cell viability at 90% for up to 4.5 hrs; however, it is widely accepted that the cells form higher quality seals if used within 45 minutes of passaging.[21]

Device set-up

Prior to use, we cleaned the chips overnight with a piranha solution consisting of 3:1 (v/v) concentrated sulphuric acid and 30% (v/v) aqueous hydrogen peroxide solution at 90 °C. Immediately preceding each experiment, we rinsed a chip with Milli-Q water, dried it with argon gas, and mounted it in the scaffold shown in Fig. 3a-b. We placed the scaffold on a vibration isolation table (BM-4, Minus K Technology) inside of a Faraday cage to minimize noise. A constant-pressure pump (Suction Control Pro, Nanion) and shutoff valve were located upstream and downstream of each pore, respectively. To fill the pores with solution, we applied positive pressure while the shutoff valves were open. Once the L-shaped channels (Fig. 2c) were filled, as indicated by a significant decrease in the flow rate, we closed both shutoff valves to stop perfusion and placed solution in the well above the chip. The fluidic resistance of each pore is relatively high in comparison to that of the L-shaped channels; hence, the amount of time needed to fill the scaffold can be dramatically reduced by allowing air to flow out the downstream end of each L-shaped channel before solution reaches the chip. An Ag/AgCl electrode located upstream of the recording pore served as the command electrode, which we attached to the headstage of a patch-clamp amplifier (EPC 10 Plus, HEKA), while a second electrode in the bath solution served as ground. We used commercially available software for data acquisition (PatchMaster, HEKA).

Patch-clamp experiments

We filled the recording and positioning pores with an electrolyte solution consisting of 140 mM KCl, 5 mM NaCl, 10 mM HEPES, 5 mM glucose, 2 mM $CaCl_2$, and 2 mM $MgCl_2$ (pH = 7.4). After filling each pore, we applied a positive pressure of 3 kPa to the recording pore until we attempted to establish a seal. After adding cells to the well above the chip, we applied a negative pressure of -2.5 kPa to the positioning pore to aspirate a cell (Fig. 3c). During this process, we regularly applied a 10 mV voltage pulse to monitor the resistance across the recording pore. Once a significant increase in resistance was observed, we immediately applied a negative pressure of -3 kPa to the recording pore and stopped applying pressure to the positioning pore (Fig. 3c). If the seal resistance stabilized for a prolonged duration (> 15 s) prior to reaching the gigaohm range, we gradually increased the magnitude of the negative pressure up to a maximum of -30 kPa. Once we established a gigaseal, we ceased to apply pressure to either pore. We obtained all recordings in the cell-attached configuration and voltage-clamp mode (*i.e.* at constant applied potential). We set the low-pass 4-pole Bessel filter of the amplifier to a cut-off frequency of 5 kHz and used a sampling rate of 25 kHz.

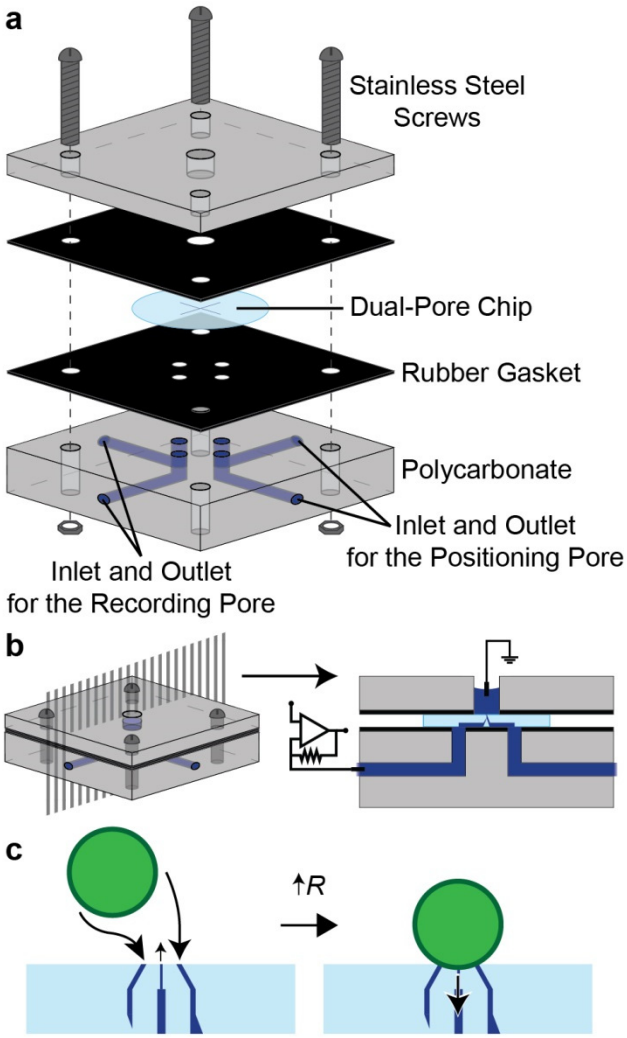

Fig. 3 Using a dual-pore glass chip in a planar patch-clamp experiment. (**a**) Schematic showing the assembly of the scaffold used to interface with a dual-pore chip. We oriented the chip such that the low-resistance L-shaped channels (Fig. 2c) were facing downward. The ends of these channels were continuous with channels in the polycarbonate, providing two separate flow paths for perfusing to each pore. (**b**) Assembled scaffold; the cross-section shown on the right corresponds to the plane indicated on the left. (**c**) Simplified representation of the strategy used to establish a high-resistance seal with a cell. Briefly, we applied suction to the positioning pore and positive pressure to the recording pore until we detected an increase in resistance resulting from a cell being positioned in the vicinity of the recording pore. At this point, we ceased to apply suction to the positioning pore and applied suction to the recording pore to establish a seal.

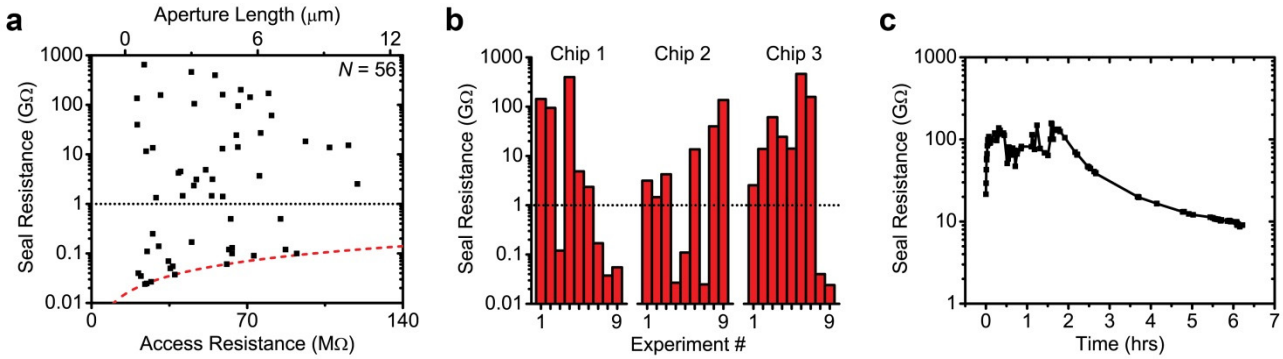

Fig. 4 Dual-pore chips repeatedly form and maintain seals in patch-clamp experiments with HEK-293 cells. (**a**) Maximum seal resistance versus access resistance and estimated length of the single-shot aperture (Fig. 2a). We excluded experiments in which the access resistance was significantly larger (> 10%) than what we previously measured. The red dashed line corresponds to no change in the seal resistance during an experiment and the black dotted line indicates a seal resistance of 1 GΩ. (**b**) Ability of the same chip to repeatedly form gigaseals. We used each chip in nine patch-clamp experiments. Between experiments, we cleaned the chips in 1% Micro-90 and piranha solution. Chips 1, 2, and 3 formed gigaseals in 56, 67, and 78 percent of the experiments, respectively. The black dotted line indicates a seal resistance of 1 GΩ. (**c**) Maintaining a gigaseal for a prolonged duration. We were able to maintain a gigaseal for over 6 hrs using a dual-pore chip. The seal resistance reached its maximum value of 154 GΩ at approximately 1.6 hrs into the experiment. We measured all seal resistances while in the cell-attached configuration.

After use in a patch clamp experiment, each chip was placed in a solution of 1% Micro-90 (International Products Corporation), an alkaline cleaning solution that is used to remove biological debris, and desiccated for roughly 30 minutes to ensure the pores were filled with the solution. The chips were kept in this solution until they were cleaned in piranha for additional experiments.

Results and discussion

Device characterization

As dual-pore glass chips (Fig. 2b-c) cannot be machined using traditional microfabrication techniques, we used femtosecond laser ablation to fabricate our design in borosilicate glass coverslips. Herbstman and Hunt had previously shown that high-aspect ratio nanochannels can be machined by focusing a single femtosecond laser pulse just below the surface of a glass coverslip.[38] We used this technique to fabricate the opening of the recording pore (Fig. 2a), then used high-repetition-rate ablation to machine the rest of the geometry. Fig. 2d shows a scanning electron microscopy (SEM) image of the surface of a completed dual-pore chip. Due to differences between single-shot and high-repetition-rate ablation, the recording pore is smoother than the positioning pore; in fact, the recording pore appears devoid of discernable roughness, similar to the tip of a patch pipette. Smoother pores tend to yield higher seal resistances, highlighting the importance of using single-shot ablation to machine the recording pore.[39] The recording pore is also smaller in diameter than a typical planar patch-clamp pore and hence is better suited for forming high-resistance seals due to geometric factors.[8]

We characterized the resistance of the recording pore in series with the L-shaped channel (*i.e.* the access resistance) using a standard extracellular solution ($\rho \sim 0.5\ \Omega$ m). The resistance varied between 24 and 116 MΩ with an average value of 60 ± 25 MΩ (N = 18 chips). While these resistances are generally too large for whole-cell recordings without using series resistance compensation, they are suitable for cell-attached single-channel recordings. Assuming the diameter of the single-shot aperture (Fig. 2a) is constant at 250 nm, these resistances suggest that the aperture typically accounts for the majority of the access resistance (78%) and that its length varies between 1 to 10 μm and is 5 ± 2 μm on average (see Supplementary Section S4). Based on the dimensions shown in Fig. 2b-c, we expect the resistance of the positioning pore in series with the L-shaped channel to be less than 2 MΩ, which is similar to the resistance of other planar patch-clamp pores that use suction to position a cell.[10–12] Hence, we expect the positioning pore to be able to position a cell as effectively as these other devices.

Low capacitance is critical for minimizing dielectric noise and the distributed *RC*-noise of the recording pore. Therefore, we determined the total capacitance of the recording setup by cancelling the fast capacitive transients that occur upon the application of a voltage pulse. On average, we measured a capacitance of 1.8 ± 0.4 pF (N = 39; see Supplementary Section S5 for a boxplot of this data). The amplifier and headstage contribute 1 to 1.5 pF to this capacitance, which indicates that the polycarbonate scaffold, electrode leads, and dual-pore chip contribute approximately 0.3 to 0.8 pF in total. The combined capacitance of the scaffold, leads, and chip is comparable to the lowest values reported in the literature for other planar patch-clamp devices and is smaller than the capacitance of a typical patch pipette.[10,11] In order to achieve such a low capacitance, we found that it was crucial to minimize the length of the electrode leads and to interface with the backside of each pore *via* a microchannel (Fig. 2c).

Seal quality

High seal resistances are critical for providing high fidelity single-channel recordings with minimal noise and leakage currents. To assess the ability of the dual-pore chips to establish high-resistance seals, we conducted planar patch-clamp

experiments with HEK-293 cells using the seal formation strategy shown in Fig. 3c. In over 90 percent of the experiments, we observed a significant increase in resistance (*i.e.* greater than ~5% of the access resistance), indicating that a cell was positioned in the vicinity of the recording pore. Typically, this increase in resistance occurred within 1 to 2 minutes after adding cells. Fig. 4a shows the maximum seal resistance we obtained in each experiment with respect to the access resistance and estimated length of the single-shot aperture (Fig. 2a). While Nagarah *et al.* previously observed a positive correlation between seal resistance and pore length with quartz pores, we observed no such correlation in this work (Pearson's r = -0.10).[12] This discrepancy may result from the relatively small diameter of the recording pore, which could reduce the protrusion of the membrane into the pore upon the application of suction. Nonetheless, the rate of gigaseal formation was 61 percent, the mean seal resistance was 53 GΩ, the median seal resistance was 3 GΩ, and the maximum seal resistance was 650 GΩ. Excluding experiments in which we did not form a gigaseal, the mean and median seal resistances were 87 and 15 GΩ, respectively. Whereas the rate of gigaseal formation is comparable to that of other planar patch-clamp devices, the magnitude of the seal resistance is relatively large when a gigaseal is formed.[10] For instance, van Stiphout *et al.* obtained a median gigaseal resistance of approximately 2 GΩ using the CytoPatch device.[15] In certain cases, a gigaseal may have failed to form as a result of off-center positioning of the cell; this is supported by the observation that the initial increase in resistance upon positioning a cell tended to be lower when a gigaseal did not form.

Fig. 4b shows that the same dual-pore chip can be used to form a gigaseal on multiple occasions by cleaning the chip between experiments (see Experimental section for details). Seal resistance was not clearly correlated with the number of times we used each chip (Pearson's r = -0.43, 0.67, and 0.17), suggesting that the same chip can be re-used indefinitely without degrading the average seal quality. Kao *et al.* obtained a similar result using a slightly different cleaning procedure with the Nanion Port-a-Patch system.[40] Consequently, it might be possible to improve the rate of gigaseal formation and average seal resistance in future experiments by re-using only the best-performing dual-pore chips (*e.g.* Chip 3 in Fig. 4b).

Finally, Fig. 4c shows the seal resistance from a single patch-clamp experiment as a function of time. We were able to maintain a gigaseal for over 6 hrs, which is long in comparison to the typical duration of a conventional patch-clamp experiment performed in the cell-attached configuration. Prolonging the duration of a gigaseal permits longer recordings that ultimately increase data throughput *via* the exploration of a wider parameter space; accordingly, a platform such as the one presented here that is capable of maintaining a seal for an extended duration is ideal for maximizing the utility of each experiment.

Noise characterization

From experiment to experiment, the root-mean-square (RMS) current (*i.e.* noise) we measured after forming a gigaseal with a dual-pore chip varied between 0.46 to 1.3 pA and was 0.92 pA on average at a bandwidth of 5 kHz and an applied potential of ±50 mV (N = 13; see Supplementary Section S6 for a boxplot of this data). To our knowledge, the lowest RMS current ever reported for a planar patch-clamp platform in the cell-attached configuration is 0.27 pA at a bandwidth of 1 kHz.[11] Here, we achieved RMS currents as low as 0.12 pA at 1 kHz bandwidth. Using a conventional patch-clamp setup, the RMS current varied between 0.48 to 0.83 pA and was 0.58 pA on average under the same conditions as used with the dual-pore chip (N = 6; see Supplementary Section S6 for a boxplot of this data). While the average RMS current of the dual-pore platform is approximately 60 percent higher than that of the conventional setup, the minimum noise values achieved by both platforms are nearly identical. Furthermore, nearly 40 percent of the experiments conducted with the dual-pore platform achieved levels of noise that fell within the range observed for the conventional setup. Hence, the platform developed here was often able to perform as well as a conventional patch-clamp setup after establishing a gigaseal.

The RMS current generated by the headstage, analog low-pass Bessel filter, amplifier, and digitizer was approximately 0.15 pA at a bandwidth of 5 kHz. The additional noise observed during a patch-clamp experiment was likely dominated by the distributed RC-noise of the recording pore since other sources of noise (i.e. dielectric and Johnson noise) should be relatively small according to theory.[41] To reduce this noise, the access resistance of the recording pore could be reduced by, for example, increasing the depth of the L-shaped channel leading to the pore (Fig. 2c). This was attempted but increasing the depth made the chips too fragile to handle easily.

Cell-attached single-channel recordings

To demonstrate the capability of the dual-pore platform to perform cell-attached single-channel recordings with similar fidelity to the conventional method, we performed patch-clamp experiments with HEK-293 cells that were transfected with large-conductance Ca^{2+}-activated K^+ (BK) channels. We used an extracellular solution with a high concentration of potassium (140 mM) for these experiments to establish a resting membrane potential that was near zero. Fig. 5 shows the resulting single-channel recordings obtained using the dual-pore platform as well as a conventional patch-clamp setup (see Supplementary Section S7 for additional current traces). In each experiment, we could clearly distinguish two levels of current. We measured a single-channel conductance of 203 and 253 pS using the dual-pore and conventional setups, respectively. These two values are both within the expected range for BK channels (100 to 270 pS) and are in fairly good agreement with each other (22% difference).[42] Furthermore, the RMS noise varied by less than 5 percent between the two experiments. These results show that the dual-pore platform is

capable of performing low-noise single-channel recordings in the cell-attached configuration that are comparable to those obtained using the conventional technique.

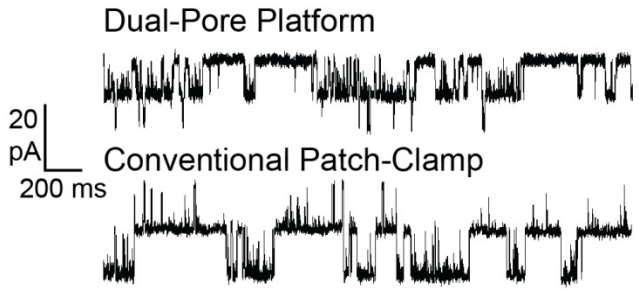

Fig. 5 Comparison of cell-attached single-channel recordings obtained using the dual-pore platform and a conventional patch-clamp setup. The activity of single BK channels was monitored at a bandwidth of 5 kHz (as plotted) and an applied potential of -50 mV. The seal resistance was in excess of 10 GΩ in both experiments. The RMS current in the absence of single-channel activity was 0.95 and 0.90 pA at 5 kHz bandwidth for the dual-pore and conventional setup, respectively.

Conclusions

Even with the advent of automated planar patch-clamp platforms, the conventional micropipette-based technique is still the method of choice for performing cell-attached single-channel recordings largely due to the high signal-to-noise ratios that are required. Here, we developed dual-pore glass chips designed explicitly for performing such recordings in an automated manner. By employing a dual-pore design, we were able to use a patch aperture that is much smaller than a typical planar patch-clamp pore and hence better-suited for forming high-resistance seals without sacrificing the ability of the device to position a cell *via* suction. Glass is an ideal substrate for planar patch-clamp due to its excellent dielectric and seal forming properties; however, it is difficult to fabricate complex three-dimensional structures, such as the design described here, in glass *via* conventional microfabrication techniques. Only laser-based machining as used here makes it possible to fabricate such structures in glass. Using the dual-pore platform, we achieved exceptionally high seal resistances and the lowest noise ever reported in the cell-attached configuration for a planar platform. Furthermore, we obtained single-channel recordings with similar fidelity to the gold standard (*i.e.* conventional) technique. Ideally, the dual-pore platform developed here will inspire future designs for performing high-throughput screening of single ion channels and help to expedite the drug discovery process by providing information that is complementary to whole-cell recordings. In future work, the design described here could be modified to accommodate smaller cells and organelles by using an array of single-shot pores for positioning instead of one or two large pores. In addition, two sets of dual-pores could be fabricated in close proximity to one another for performing automated on-chip gap junction recordings.

Acknowledgements

The authors thank H. Wulff for the HEK-293 cell line. This work was supported by the National Science Foundation (M.M., EFRI-BSBA, 0937323) and the National Institutes of Health (M.M., NIH Shared Instrumentation Program, S10-RR-025592; M.M., NIH-R01, NIGMS, 1R01GM091705-01).

Notes and references

[a] Department of Biomedical Engineering, University of Michigan, Ann Arbor, MI 48109, USA
[b] Center for Ultrafast Optical Science, University of Michigan, Ann Arbor, MI 48109, USA
[c] Department of Chemical Engineering, University of Michigan, Ann Arbor, MI 48109, USA

† Electronic Supplementary Information (ESI) available: Supplementary Sections S1 through S7 and Supplementary Figures S1 through S4. See DOI: 10.1039/b000000x/

‡ Dedicated *in memoriam* to Alan J. Hunt

1. W. Zheng and L. Kiss, *Am. Pharm. Rev.*, 2003, **6**, 85–92.
2. C. V. Remillard and J. X. J. Yuan, *Conventional Patch Clamp Techniques and High-Throughput Patch Clamp Recordings on a Chip for Measuring Ion Channel Activity*, Springer, New York, 2011.
3. G. C. Terstappen, R. Roncarati, J. Dunlop, and R. Peri, *Future Med. Chem.*, 2010, **2**, 715–730.
4. A. Mathie, *J. Pharm. Pharmacol.*, 2010, **62**, 1089–1095.
5. A. Wickenden, B. Priest, and G. Erdemli, *Future Med. Chem.*, 2012, **4**, 661–679.
6. M. Martina, *Front. Pharmacol.*, 2012, **3**, 86.
7. E. Neher and B. Sakmann, *Nature*, 1976, **260**, 799–802.
8. *Single-Channel Recording*, Plenum Press, New York, 2nd edn., 1995.
9. M. Mortensen and T. G. Smart, *Nat. Protoc.*, 2007, **2**, 2826–2841.
10. C. Y. Chen, T. Y. Tu, C. H. Chen, D. S. Jong, and A. M. Wo, *Lab. Chip*, 2009, **9**, 2370–2380.
11. N. Fertig, M. Klau, M. George, R. H. Blick, and J. C. Behrends, *Appl. Phys. Lett.*, 2002, **81**, 4865–4867.
12. J. M. Nagarah, E. Paek, Y. Luo, P. Wang, G. S. Hwang, and J. R. Heath, *Adv. Mater.*, 2010, **22**, 4622–4627.
13. E. Stava, M. R. Yu, H. C. Shin, and R. H. Blick, *Ieee Trans. Nanobioscience*, 2010, **9**, 307–309.
14. E. Stava, M. R. Yu, H. C. Shin, H. Shin, J. Rodriguez, and R. H. Blick, *Lab. Chip*, 2012, **12**, 80–87.
15. P. van Stiphout, T. Knott, T. Danker, and A. Stett, *Mikrosystemtechnik Kongr.*, 2005, 435–438.
16. A. Boussaoud, I. Fonteille, G. Collier, F. Kermarrec, F. Vermont, E. Tresallet, M. De Waard, C. Arnoult, and N. Picollet-D'hahan, *Biosens. Bioelectron.*, 2012, **32**, 96–103.
17. C. Py, M. W. Denhoff, M. Martina, R. Monette, T. Comas, T. Ahuja, D. Martinez, S. Wingar, J. Caballero, S. Laframboise, J. Mielke, A. Bogdanov, C. Luk, N. Syed, and G. Mealing, *Biotechnol. Bioeng.*, 2010, **107**, 593–600.
18. S. Pandey, R. Mehrotra, S. Wykosky, and M. H. White, *Solid-State Electron.*, 2004, **48**, 2061–2066.

19. B. Matthews and J. W. Judy, *J. Microelectromechanical Syst.*, 2006, **15**, 214–222.
20. Z. L. Zhang, T. Asano, H. Uno, R. Tero, M. Suzui, S. Nakao, T. Kaito, K. Shibasaki, A. Tominaga, Y. Utsumi, Y. L. Gao, and T. Urisu, *Thin Solid Films*, 2008, **516**, 2813–2815.
21. T. Sordel, F. Kermarrec, Y. Sinquin, I. Fonteille, M. Labeau, F. Sauter-Starace, C. Pudda, F. de Crecy, F. Chatelain, M. De Waard, C. Arnoult, and N. Picollet-D'hahan, *Biomaterials*, 2010, **31**, 7398–7410.
22. T. Lehnert, M. A. M. Gijs, R. Netzer, and U. Bischoff, *Appl. Phys. Lett.*, 2002, **81**, 5063–5065.
23. J. M. Nagarah, P. Wang, Y. Luo, R. Pantoja, N. A. Melosh, D. M. Starace, R. Blunk, F. Bezanilla, and J. R. Heath, *Biophys. J.*, 2005, **88**, 522A–522A.
24. P. Weerakoon, E. Culurciello, Y. S. Yang, J. Santos-Sacchi, P. J. Kindlmann, and F. J. Sigworth, *J. Neurosci. Methods*, 2010, **192**, 187–192.
25. C. Schmidt, M. Mayer, and H. Vogel, *Angew. Chem. Int. Ed Engl.*, 2000, **39**, 3137–3140.
26. B. J. Xu, Z. B. Liu, Y. K. Lee, A. Mak, and M. Yang, *Sens. Actuators -Phys.*, 2011, **166**, 219–225.
27. K. G. Klemic, J. F. Klemic, M. A. Reed, and F. J. Sigworth, *Biosens. Bioelectron.*, 2002, **17**, 597–604.
28. K. G. Klemic, J. F. Klemic, and F. J. Sigworth, *Pflugers Arch.-Eur. J. Physiol.*, 2005, **449**, 564–572.
29. A. Y. Lau, P. J. Hung, A. R. Wu, and L. P. Lee, *Lab. Chip*, 2006, **6**, 1510–1515.
30. X. H. Li, K. G. Klemic, M. A. Reed, and F. J. Sigworth, *Nano Lett.*, 2006, **6**, 815–819.
31. A. Stett, V. Bucher, C. Burkhardt, U. Weber, and W. Nisch, *Med. Biol. Eng. Comput.*, 2003, **41**, 233–240.
32. D. Martinez, C. Py, M. W. Denhoff, M. Martina, R. Monette, T. Comas, C. Luk, N. Syed, and G. Mealing, *Biomed. Microdevices*, 2010, **12**, 977–985.
33. S. Tanzi, M. Matteucci, T. L. Christiansen, S. Friis, M. T. Christensen, J. Garnaes, S. Wilson, J. Kutchinsky, and R. Taboryski, *Lab. Chip*, 2013, **13**, 4784–4793.
34. M. Estacion, J. S. Choi, E. M. Eastman, Z. Lin, Y. Li, L. Tyrrell, Y. Yang, S. D. Dib-Hajj, and S. G. Waxman, *J. Physiol.-Lond.*, 2010, **588**, 1915–1927.
35. C. Wood, C. Williams, and G. J. Waldron, *Drug Discov. Today*, 2004, **9**, 434–441.
36. A. Lepple-Wienhues, D. Lassen, A. Hummer, U. Czubayko, M. Knirsch, and A. Golubovic, *Comb. Chem. High Throughput Screen.*, 2009, **12**, 73–77.
37. K. Ke, E. Hasselbrink, and A. J. Hunt, 2005, vol. 5714, pp. 53–62.
38. J. F. Herbstman and A. J. Hunt, *Opt. Express*, 2010, **18**, 16840–16848.
39. M. Malboubi, Y. Gu, and K. Jiang, *Microelectron. Eng.*, 2010, **87**, 778–781.
40. L. Kao, N. Abuladze, X. M. Shao, K. McKeegan, and I. Kurtz, *J. Neurosci. Methods*, 2012, **208**, 205–210.
41. J. D. Uram, K. Ke, and M. Mayer, *ACS Nano*, 2008, **2**, 857–872.
42. L. Salkoff, A. Butler, G. Ferreira, C. Santi, and A. Wei, *Nat. Rev. Neurosci.*, 2006, **7**, 921–931.

